Journal of Electroanalytical Chemistry 981 (2025) 118961

Contents lists available at ScienceDirect

Journal of Electroanalytical Chemistry

journal homepage: www.elsevier.com/locate/jelechem

Development of free-standing h-BN/rGO/S composite cathodes for Li-S batteries: h-BN content and temperature effect

Ayşe Şahin [a], Hilal Günsel [b,*], Şeyma Dombaycıoğlu [c,d], Ali Osman Aydın [e]

[a] Sakarya University Institute of Natural Sciences Department of Chemistry Sakarya Turkiye
[b] Sakarya University of Applied Sciences Faculty of Technology Department of Engineering Fundamental Sciences Sakarya Turkiye
[c] Sakarya University Faculty of Science Department of Chemistry Sakarya Turkiye
[d] Sakarya University Research Development and Application Center (SARGEM) Sakarya Turkiye
[e] İstanbul Medipol University Faculty of Pharmacy Department of Basic Pharmaceutical Sciences İstanbul Turkiye

ARTICLE INFO

Keywords:
h-BN/rGO/S composite cathodes
h-BN content
Temperature effect
Free-standing papers
Li-S batteries

ABSTRACT

This study aims to improve the properties of Li-S batteries and overcome their disadvantages by utilizing hexagonal boron nitride (h-BN) nanocomposites with unique features that provide advantages in their applications. For this purpose, composite films were produced using h-BN with superior mechanical and chemical properties along with reduced graphene oxide (rGO) possessing high electrical conductivity. Free-standing and flexible h-BN/rGO/S composite paper electrodes containing different weight ratios of functionalized h-BN were prepared. The obtained binder-free composite papers were employed as cathodes in Li-S batteries and applied at different temperatures. In this study, the structural, morphological, and thermal analyses of the composite cathodes were conducted using X-ray diffraction (XRD), field emission gun scanning electron microscopy (FEG-SEM), energy dispersive X-ray spectroscopy (EDS), transmission electron microscopy (TEM) and thermogravimetric analysis (TGA). The optical measurements were carried out by Fourier transform infrared spectroscopy (FT-IR), Raman spectroscopy and ultraviolet–visible spectroscopy (UV–Vis). After assembling CR2032 button cells, electrochemical performance tests were applied to assess the charge–discharge capacities. A high discharge capacity of 427 mAh g^{-1} was achieved after 1000 cycles. As a result, h-BN/rGO-based composites have been developed as environmentally friendly and metal-free materials, further enhancing the electrochemical performance and electron transport of lithium batteries.

1. Introduction

Considering the current technological advancements, the importance of stored energy has significantly increased. While lithium batteries offer advantages such as high energy density and eco-friendliness, they also come with certain disadvantages. Among these disadvantages are degradation at high temperatures, the need for protective circuits, and capacity loss due to overcharging or thermal degradation. In many studies aimed at avoiding these disadvantages, hexagonal boron nitride (h-BN) plays a significant role [1–3].

Li-S batteries have several advantages compared to others, including higher specific capacity, smaller size, higher energy density (2500 Wh kg^{-1}), and higher theoretical capacity (1672 mAh g^{-1}) [4]. Additionally, sulfur, the cathode active material, offers advantages such as being inexpensive, abundant, non-toxic, and providing high theoretical capacity and good cycling stability among its benefits. However, in Li-S batteries, lithium sulfides exhibits poor electrical conductivity. During charge–discharge cycles, soluble polysulfides form and migrate between electrodes, affecting the electrochemical performance of the battery and leading to rapid capacity loss. Lithium dendrites can penetrate the separator, causing short circuits and potentially resulting in battery ignition or explosion [1,5–8]. To address issues such as the transfer resistance caused by soluble polysulfides and the shuttle effect in Li-S batteries, various anode, cathode composites, layered structures and separators are being designed and fabricated [7,9–12].

Despite being a natural material, boron nitride possesses many superior properties. These include high thermal shock resistance, thermal conductivity, chemical stability, and lubricity. Due to these properties, it is used in various forms such as powder, shaped masses, spray, and paste in high-temperature applications in metallurgy, the electrical and

* Corresponding author.
E-mail address: hkose@subu.edu.tr (H. Günsel).

https://doi.org/10.1016/j.jelechem.2025.118961
Received 5 December 2024; Received in revised form 19 January 2025; Accepted 25 January 2025
Available online 27 January 2025

electronics industries, the ceramic industry, the production of composite materials, and the chemical industry. It also holds potential for new applications due to its advantageous properties [2,13]. Boron nitride is a boron-nitrogen compound characterized by interatomic covalent bonds and intermolecular van der Waals interactions [14]. Hexagonal boron nitride shares the same lattice structure and electron count as carbon atoms and contains a ringed and layered structure similar to graphite. However, the structural similarity of h-BN to the graphite allotrope has led to its designation as graphitic boron nitride or white graphite [15].

Functionalized boron nitrides (FBNs) have significant potential for cathode applications in energy storage devices, such as solid-state batteries. Due to their open surfaces, rapid ionic diffusion with Li, Na, and Mg ions is possible. In functionalized versions of 2D hexagonal boron nitride (h-BN), ions can diffuse very quickly, enabling fast charging and discharging of the related electrochemical energy storage devices. Additionally, because functionalized h-BN is an excellent ionic conductor, it represents simultaneous ionic and electrical conductivity, which is highly desirable for solid-state batteries, potentially addressing safety and performance issues [16]. In a study on the safety of lithium-ion batteries, it was indicated that the cell could short circuit in high temperature and high current environments. Chen et al. used boron nitride nanotubes (BNNTs) in the production of the separator, which is crucial for thermal stability, to prevent short circuits. This new BNNT separator offered enhanced thermal stability up to 150 °C, ensuring the safe operation of Li-ion battery cells at high temperatures [17]. Yang et al. designed a thin and selective interlayer structure by coating the cathode surface with a thin film of functionalized boron nitride nanolayer and graphene to mitigate the issue of rapid capacity decay caused by the shuttle effect of soluble polysulfides, which remains a major obstacle for practical applications. This approach significantly increased the specific capacity and cycle stability of Li-S batteries over a long lifespan. At the end of the study, a specific capacity of 1100 mAh g^{-1} at 3C and a low cycle decay rate of up to 0.0037 % per cycle were observed. It was stated that this new interlayer is a promising approach to significantly enhance the performance of Li-S batteries [7]. In lithium-sulfur batteries, h-BN applications have typically focused on mitigating the shuttle effect of polysulfides and reducing dendritic effects to enhance capacity. h-BN also exhibits the ability to adsorb polysulfides [4,7,18,19]. In this study, the superior mechanical and chemical properties of hexagonal boron nitride (h-BN) were combined with layered and conductive reduced graphene oxide (rGO) to mitigate the shuttle effect. The production of free-standing, flexible and binder-free cathodes in Li-S batteries was achieved by decorating elemental sulfur and h-BN between rGO layers.

2. Experimental

2.1. Procedure

Production of h-BN/rGO/S composite films was achieved by decorating elemental sulfur and h-BN between rGO layers. To accomplish this, h-BN underwent prior functionalization. Subsequently, graphite oxide was produced from graphite using the modified Hummers method [20]. The h-BN used in the study (Aldrich, 98 %) was commercially purchased, while elemental sulfur (Alfa Aesar, 99.5 %) was employed as the active cathode material in Li-S batteries. After graphene oxide production via the Hummers method, h-BN/rGO/S composites were prepared as free-standing and flexible paper electrodes with sulfur content of at least 50 % by weight and h-BN content ranging from 0 %, 5 %, 10 %, to 15 % by weight. These composite materials were used as electrodes in Li-S batteries. To achieve this, homogeneous suspensions of the composites were prepared using ultrasonication, and flexible electrodes in paper form were obtained via vacuum filtration.

In the initial stage, efforts were focused on the functionalization of h-BN to ensure its homogenization for electrode production. Based on the characterization and homogenization processes, an appropriate method was determined. Chemical processes used to produce graphene oxide (GO) cannot be applied to hexagonal boron nitride (h-BN) due to its high resistance to oxidation. Studies have shown that when high-temperature heat treatment (900 °C) is applied to h-BN in an oven under ambient air, oxygen is incorporated into the h-BN lattice, resulting in a mass gain [21]. Before this process, despite using water bath sonication to increase the rate of suspension formation, homogeneous dispersion was not achieved. However, after this heat treatment, simply stirring the material in deionized water for a few minutes without the need for sonication easily facilitated suspension formation.

In the second stage, the production of graphite oxide from graphite was carried out using a modified Hummers method, as commonly described in the literature, for the fabrication of h-BN/rGO/S composite flexible paper electrodes [20]. The obtained graphene oxide (GO) was subjected to ultrasonication in pure ethyl alcohol (1 mg/mL). After dispersing GO in ethanol, 0.1 mL of aqueous hydrazine solution was added to the ultrasonication medium to reduce GO to reduced graphene oxide (rGO) form. After further processing, h-BN was added in different weight ratios and suspended. In the final step of ultrasonication, elemental sulfur was added, and ultrasonication continued for 2 h. The resulting homogeneous suspension was filtered through a PvDF membrane filter (0.22 μm pore size) via vacuum filtration to produce flexible and free-standing h-BN/rGO/S composite films in paper form. Consequently, h-BN/rGO/S composite paper electrodes with h-BN content of 0 %, 5 %, 10 %, and 15 % by weight were prepared for use as cathodes in Li-S batteries. These cathodes were respectively coded as 0 h-BN, 5 h-BN, 10 h-BN, and 15 h-BN. In the final step, the produced h-BN/rGO/S composite papers were annealed at 155 °C for 2 h to allow elemental sulfur to melt and penetrate between the layers.

2.2. Characterization of the materials

In this study, functionalization of h-BN was carried out to ensure its homogeneous distribution in electrode production, and then the produced h-BN/rGO/S nanocomposite papers was used as cathodes in the battery. Initially, the functionalization of h-BN was confirmed using FT-IR spectroscopy (Spectrum Two model PerkinElmer FT-IR). The composite structure and its components were investigated by Raman spectroscopy (RAMANRXN SYSTEMS). Morphological analyses of the cathodes were conducted using FEI QUANTA 450 model FEG-SEM and high resolution mode of JEOL JEM-1220 model TEM devices. Elemental mapping was applied to determine the distribution of the contents by EDS attached to the FEG-SEM. The crystal structure of the composites was examined via XRD (Rigaku D/MAX/2200/PC model device) using CuKα radiation (λ = 1.54050 Å) with 2°/min scanning speed. TGA was carried out with the Netzsch STA 449 F1 Jupiter model thermal analyzer at the heating rate of 10 °C/min under N_2 atmosphere. h-BN effect on the polysulfide adsorption was eaxmanined via UV–Vis spectroscopy (Agilent Model 8453 diode array spectrophotometer).

After assembling the CR2032 cell in a glove box (MBraun-Labstar), electrochemical performance tests were conducted to analyse the charge–discharge capacities using a BST8-MA MTI model battery tester with 0.1C cycling rate for 100 cycles between the 3.0——1.5 V. We used h-BN/rGO/S nanocomposites as cathode, metallic Li as anode and polypropylene (PP) (Celgrad 2400) as separator. As electrolyte 1 M LiTSFI and 0.1 M $LiNO_3$ solution in a mixture of 1:1 (v/v) 1,3-dioxolane (DOL) and 1,2-dimethoxyethane (DME) was used. Cyclic voltammetry (CV) and electrochemical impedance analysis (EIS) were utilized to characterize electrochemical behavior of the cathodes in the Li-S cell by OrigaFlex OGF500 model OrigaLys ElectroChem SAS. CV was carried out at the scan rate of 0.1 mVs^{-1} within the same voltage range and EIS analysis was performed in a frequency range of 1000 kHz–0.01 Hz applying a sine wave of 10 mV amplitude.

3. Results and discussion

3.1. Characterization of h-BN/rGO/S nanocomposite cathode materials

Free-standing and flexible h-BN/rGO/S composite paper cathodes containing different weight ratios of functionalized h-BN were prepared by using vacuum filtration method after ultrasonication process. The experimental stages carried out are shown in Scheme 1.

Various studies have been conducted on the functionalization of h-BN to ensure its homogeneous distribution in electrode production. We achieved the best result through functionalization at high temperature (900 °C) in air atmosphere, which was confirmed by FT-IR spectroscopy. Fig. 1 shows the FT-IR spectrum of the product compared with the pristine h-BN powder spectrum after high-temperature functionalization in a muffle furnace under air atmosphere. As seen in the figure, the spectrum of the h-BN sample after functionalization exhibits characteristic peaks of h-BN, including the stretching vibration of the B-N plane and the out-of-plane bending vibration of the B-N-B plane, observed at approximately 1300 cm^{-1} and 750 cm^{-1}, respectively. The characteristic peak of the —OH groups located on the surface and edge planes of h-BN appears as an —O—H vibration band around 3250 cm^{-1} [21].

Fig. 2(a) shows the XRD analysis of the h-BN/rGO/S composite paper cathode structure. As seen in the figure, the presence of elemental S, rGO, and h-BN peaks in the cathodes produced with different h-BN additives indicates the successful production of composite structures. The XRD peak positions of the produced h-BN/rGO/S composites mainly include S (JCPDS, 00-008-0247), h-BN (JCPDS, 00-034-0421), and carbon (JCPDS, 00-026-1080). The successful production of GO is evidenced by the characteristic plane peak observed at approximately 11° in the XRD analysis. After reduction, this peak shifts to around 26°, indicating the presence of rGO carbon peak. The S (222), C (002), and h-BN (002) lattice planes overlap at around $\theta \approx 26°$ [22]. The main peaks of S, h-BN, and carbon crystal structures are clearly observed in the composite structure.

To evaluate the thermal stability and sulfur content of the produced h-BN/rGO/S composite cathode, TGA was conducted in the range of

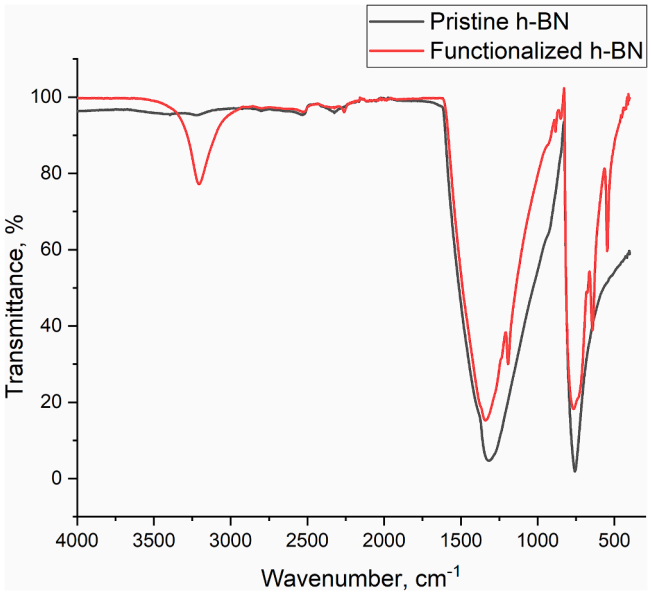

Fig. 1. FT-IR spectrum of the product after functionalization at high temperature with pristine h-BN powder spectrum.

20–500 °C under N_2 atmosphere. When examining the TG curve provided in Fig. 2(b), no weight loss was observed up to 200 °C. This is due to the absence of adsorbed water in the sample, as it underwent predrying, thus no loss occurred. The h-BN present in the composite structure exhibits high thermal stability in the studied temperature range and does not cause any weight loss [23].

Since the thermal treatment was conducted in a nitrogen atmosphere, there was no loss of carbon content in the rGO. Therefore, the decrease observed in the product is solely attributed to sulfur components. As depicted in Fig. 2(b), the weight loss in the h-BN/rGO/S composite began around 200 °C, and when the temperature reached

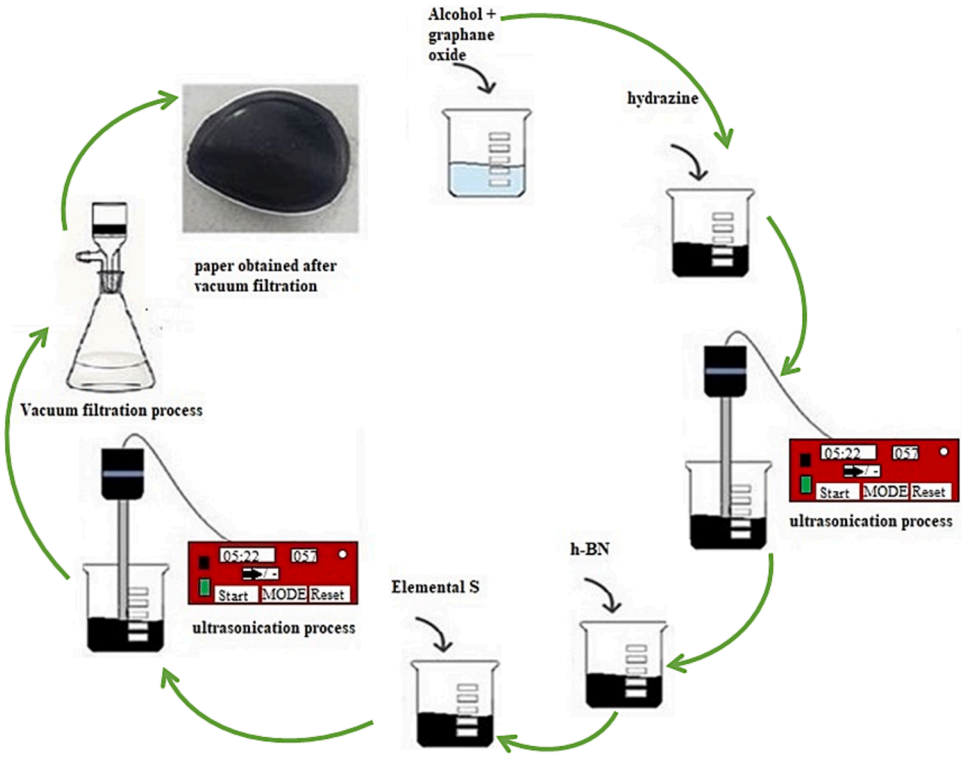

Scheme 1. Representation of the experimental stages of composite paper production.

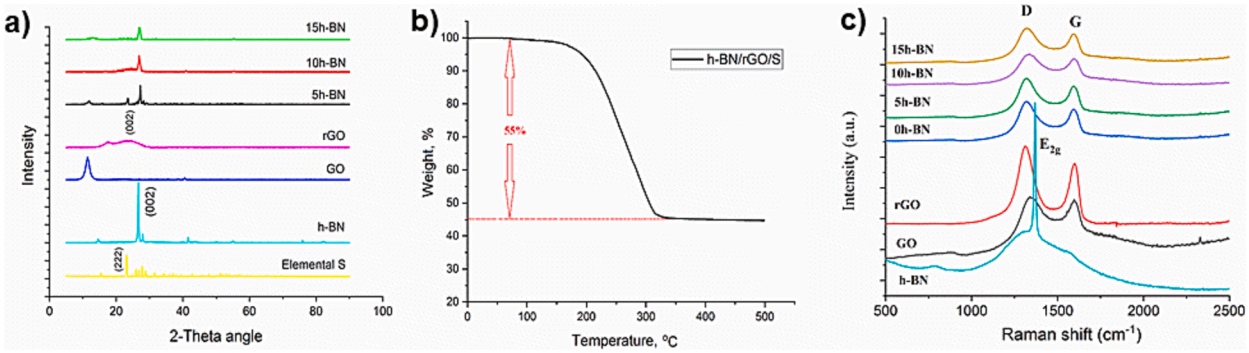

Fig. 2. a) XRD diffractograms of h-BN/rGO/S composite paper cathodes. b) TGA of h-BN/rGO/S composite paper. c) Raman analysis of GO, rGO, h-BN and h-BN/rGO/S composite structures.

around 300 °C, sulfur had completely sublimated. At this point, approximately 55 % of the total weight had been lost. According to the results obtained from TG analysis, it is evident that the targeted cathode active material content has been achieved.

The structural and electronic analyses of GO, rGO, h-BN and the composite structures were conducted via Raman spectroscopy as seen in Fig. 2(c). h-BN spectra indicates the B-N bond of E_{2g} vibrational mode at 1368 cm^{-1}. GO, rGO and h-BN/rGO/S spectra exhibit D and G bands, in which the D band is derived from defected regions or disordered carbon sources, whereas the G band is corresponding to planar vibrations of the sp^2 carbon atom pairs. Intensity ratio of D to G band (I_D/I_G) obtained from the Raman spectra of graphene based structures can be utilized to determine disorder degree [24]. I_D/I_G ratio was calculated for GO and rGO as 1.03 and 1.286, respectively. The fact that the rGO value is higher than that of GO is due to the formation of defects as a result of the reduction process of the GO structure. This supports and confirms the structural changes during the reduction process of GO. The analysis represents the D and G bands of GO at 1336 cm^{-1} and 1596 cm^{-1}, respectively. In addition to this, the rGO spectrum showed the G band approximately 1598 cm^{-1} and the red-shifted D band at 1311 cm^{-1} [25]. Because the h-BN E_{2g} peak overlaps with the D band, the I_D/I_G ratio does not supply meaningful information about the disorder degree and graphitization for h-BN/rGO/S composite structure. As a result, when compared to the h-BN peak, the D band in the h-BN/rGO/S spectra has a red shift of 50 cm^{-1} [26]. Since the characteristic bands of elemental sulfur are in the fingerprint region, the addition of S to the h-BN/rGO composites does not affect the D and the G bands of the compounds [23].

The morphology of the produced cathodes has been imaged from both surfaces and cross-sections using FEG-SEM. The chemical composition of the samples was determined using EDS attached to a FEG-SEM. Fig. 3 shows the surface and cross-section micrographs obtained with FEG-SEM, while Fig. 4 displays the results of elemental mapping with EDS. In Fig. 3(a)–(e), the surface morphology of h-BN powder and h-BN/rGO/S composite papers named as 0 h-BN, 5 h-BN, 10 h-BN, and 15 h-BN are given, respectively. Fig. 3(f)–(i) shows the cross-sectional images of 0 h-BN, 5 h-BN, 10 h-BN, and 15 h-BN, respectively. The FEG-SEM image of h-BN powder reveals an agglomerate structure consisting of spherical particles. In the FEG-SEM micrograph of 0 h-BN cathode without h-BN, the surface image of the rGO layer is clearly observed. Examination of the images of composite cathodes with h-BN addition reveals homogeneous h-BN distribution on the surface and within the mesoporous layers in cross-sections. Additionally, an increase in agglomeration is observed on the surface of the 15 h-BN sample with the highest h-BN content. Examination of the cross-sectional images in Fig. 3(f)–(i) reveals layered and porous structures, which are desired morphologies for trapping active materials and polysulfides in Li-S batteries. The image taken from the cross-section in Fig. 3(i) shows a paper thickness of 60 μm. 10 h-BN TEM image taken with high resolution mode is presented in Fig. 3(j). rGO sheets can be clearly seen from the figure. In addition, h-BN / S

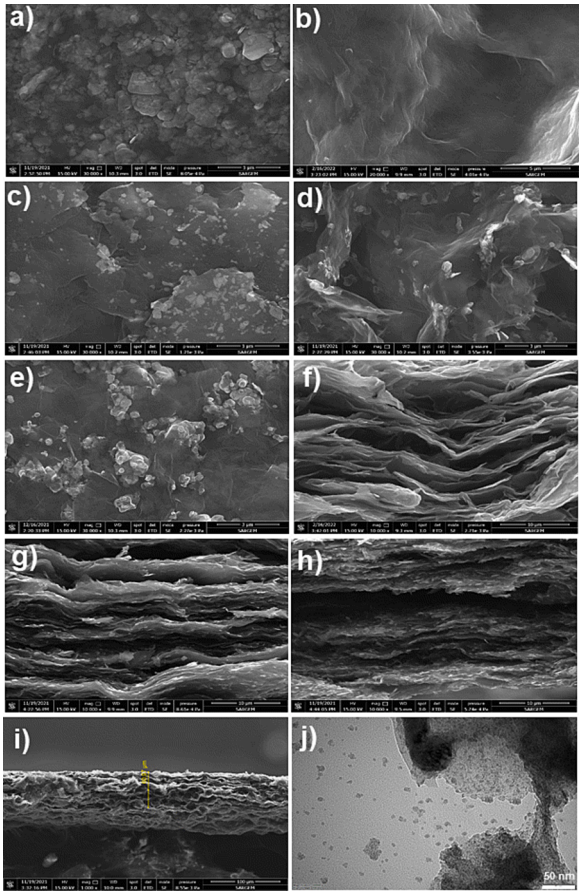

Fig. 3. (a)–(e) FEG-SEM surfaces images of h-BN powder, 0 h-BN, 5 h-BN, 10 h-BN, 15 h-BN, respectively. (f)–(i) FEG-SEM cross-section images of 0 h-BN, 5 h-BN, 10 h-BN, 15 h-BN composite papers, respectively. (j) TEM image of 10 h-BN.

incorporated into the graphene sheets is observed from the micrograph. As a result, structural and morphological studies support each other and confirm the structure of h-BN/rGO/S consisting of thermally stable h-BN and S incorporated into the conductive rGO matrix [27].

The B, N, C, and S elements present in the produced h-BN/rGO/S composite cathode are displayed with different colors in the EDS elemental mapping shown in Fig. 4. In the elemental mapping, it is seen that the components are distributed homogeneously throughout the sample section in the FEG-SEM image and the sulfur is completely absorbed into the structure. When the elemental percentages are examined, the distribution of elements and sulfur content are consistent

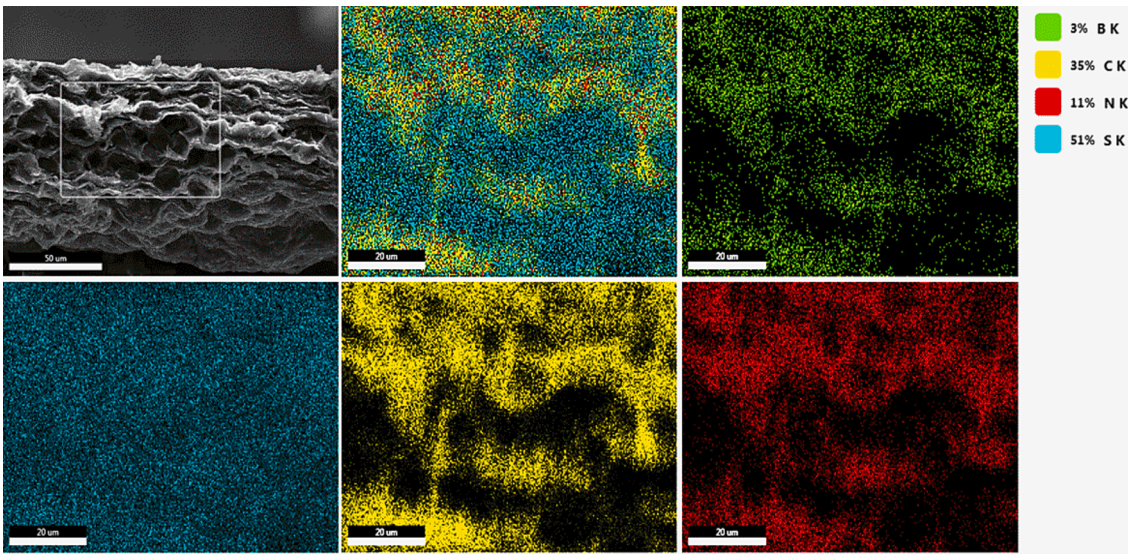

Fig. 4. EDS elemental maps of h-BN/rGO/S composite paper cathodes.

with the structure of our product.

3.2. Electrochemical performance of h-BN/rGO/S nanocomposite cathode materials

The h-BN/rGO/S composite cathodes produced in this study were fabricated into CR2032 coin cells. We utilized free-standing and flexible paper electrodes produced in this study as cathodes in the battery. Firstly, electrochemical capacity tests were conducted at room temperature within the voltage range of 1.5–3.0 V, with a cycling rate of 0.1C and 100 cycles. The change in specific discharge capacity of half-cells belonging to cathodes of without h-BN and with 5 %, 10 %, and 15 % h-BN addition, labeled as 0 h-BN, 5 h-BN, 10 h-BN, and 15 h-BN, respectively, over 100 cycles is compared in Fig. 5(a). Table 1

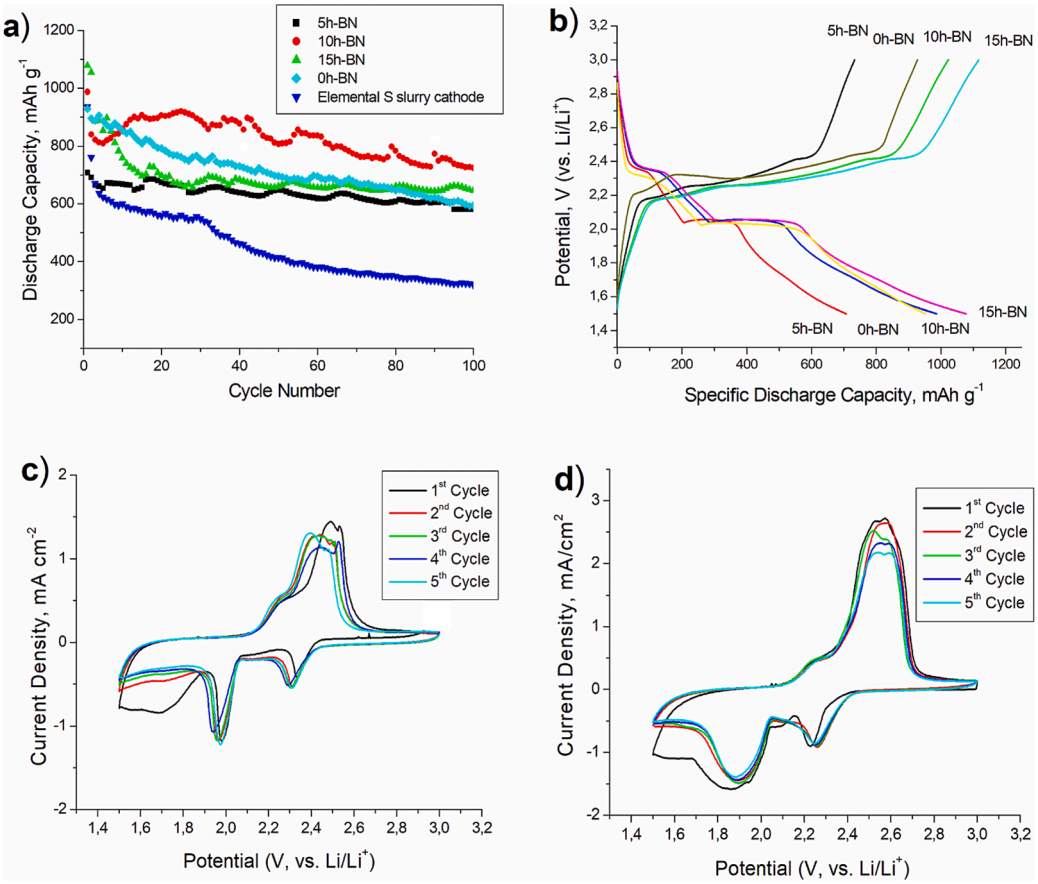

Fig. 5. a) Comparison of specific discharge capacity for composite cathodes with 0 %, 5 %, 10 %, and 15 % h-BN containing cathodes for 100 cycles at 0.1C. b) Galvanostatic charge–discharge curves of h-BN/rGO/S composite cathodes at 0.1C. Cyclic voltammograms (CV) of the samples. c) h-BN added composite cathode sample (10 h-BN). d) rGO-S cathode sample without h-BN (0 h-BN).

Table 1
Comparison of cycle capacities of composite cathodes with and without h-BN.

Sample	1st cycle, mAh g^{-1}	2nd cycle, mAh g^{-1}	50th cycle, mAh g^{-1}	100th cycle, mAh g^{-1}	Capacity Retention, %
0 h-BN	928	896	698	593	64
5 h-BN	708	691	648	581	82
10 h-BN	987	840	807	724	73
15 h-BN	1078	1055	660	645	60

summarizes the discharge capacities of h-BN-doped and undoped cathodes at the 1st, 2nd, 50th, and 100th cycles. According to the results, the 10 h-BN cathode sample with a 10 % h-BN content exhibited the highest discharge capacity after 100 cycles. During the initial discharge, cathodes with 5 %, 10 %, and 15 % h-BN additions achieved capacities of 708, 987, and 1078 mAh g^{-1}, respectively. In the second discharge, these values were 691, 840, and 1055 mAh g^{-1}, respectively. The 50th discharge yielded capacities of 648, 807, and 660 mAh g^{-1}, while the 100th discharge resulted in capacities of 581, 781, and 645 mAh g^{-1}, respectively. The undoped h-BN paper cathode provided capacities of 928 mAh g^{-1}, 896 mAh g^{-1}, 698 mAh g^{-1}, and 593 mAh g^{-1} during the 1st, 2nd, 50th, and 100th discharges, respectively. The 15 h-BN sample with the highest h-BN content initially exhibited high discharge capacity, but experienced rapid capacity decline with increasing cycle numbers, likely due to increased agglomeration on the surface and excessive h-BN content between rGO layers leading to electrical conductivity loss. As seen from the battery test results of the cathode samples, the addition of 5 % and 10 % h-BN resulted in better stability and increased capacity retention with increasing cycle numbers due to the orderly thermal distribution provided by the added h-BN content. The first cycles of galvanostatic charge–discharge curves obtained from h-BN doped and undoped cathodes, operating at a constant current density and a rate of 0.1C for 100 cycles, are compared in Fig. 5(b). These curves illustrate the potentials of reduction and oxidation reactions occurring during charge and discharge with plateaus. The discharge curves descending downwards in the figure represent reduction reactions, and the plateaus corresponding to reduction reactions are observed around 2.3 V and 2.0 V for each sample, consistent with the CV curves.

For practical utilization of batteries, electrochemical stability within the working voltage ranges is crucial [28]. Fig. 5(c) and (d) show the cyclic voltammogram (CV) curves of half-cells fabricated with h-BN doped composite cathode (10 h-BN) and rGO/S composite cathode (0 h-BN), respevtively. The CV analysis was conducted at a scan rate of 0.1 mV s^{-1} within the potential range of 1.5–3.0 V. For the Li-S battery cathode, two reduction peaks and two oxidation peaks are observed in the CV analysis. In the curve of both h-BN doped and undoped composite cathode samples, the first reduction peak is observed around 2.3 V, while the second reduction peak is around 2.0 V. The first reduction peak around 2.3 V is attributed to the formation of long-chain polysulfides (Li_2S_n, n = 4–8) from elemental sulfur (S_8) structure. The second reduction peak around 2.0 V is related to the formation of short-chain polysulfides, Li_2S_2, and Li_2S. Upon examination of the oxidation peaks, the first oxidation peak in the curve of h-BN doped composite cathode sample is observed around 2.4 V, while the second oxidation peak is seen weakly around 2.5 V. In the rGO/S composite cathode sample, the first and second oxidation peaks are observed closer to each other around 2.5 V. The first oxidation peak corresponds to the formation of Li_2S_n ($n > 2$) from Li_2S_2 / Li_2S oxidation, while the second oxidation peak is associated with sulfur formation [2]. When comparing the CV curves of the two cathodes, it can be observed that with increasing cycle numbers, polarization decreases in the curves of the h-BN doped cathode, indicating that h-BN doping enhances battery stability.

Rate capability test was also applied to 10-BN, since it has the best electrochemical performance among the other hybrid composite electrodes. The test was achieved at different current rates of 0.1C, 0.2C, 0.5C, 1C, 2C, and again 0.1C, as seen in Fig. 6(a). 10 h-BN showed specific capacity and rate performance of 857, 610, 530, 390, 200 and 661 mAh g^{-1} after each 10 cycles at current rates of 0.1C, 0.2C, 0.5C, 1C, 2C and 0.1C, respectively. When the current density is returned to 0.1C in composite cathodes, the reversible capacity provides a value close to the initial capacity. It confirms that it has stable rate performance and excellent capacity. In general, the fact that the specific discharge capacity decreases with the increase of the current rate is based on the fact that the shuttle effect increases with high current rates and damages the anode and cathode.

The electrochemical resistance of h-BN doped and undoped composite cathodes was investigated by electrochemical impedance spectroscopy. Nyquist plots obtained after completion of electrochemical charge–discharge tests are shown in Fig. 6(b). The Nyquist plots are observed as semicircles. The semicircles in the high-frequency region are expressed as charge transfer resistance (R_{ct}). When the semicircles of h-BN doped and undoped cathodes in the Nyquist plots are compared in Fig. 6(b), it is observed that the 10 h-BN cathode has lower resistance than the 0 h-BN due to the smaller semicircle. The obtained result is consistent with the electrochemical capacity values of the cathodes.

Long-term cycling perfomance of 10 h-BN was carried out at 0.5C for 1000 cycles. As seen from Fig. 6(c), the decrease in capacity was observed up to approximately 100 cycles and became stable after 100 cycles. In the first cycle, 873 mAh g^{-1} discharge capacity was obtained. In the 100th cycle, 455 mAh g^{-1} and at the end of 1000 cycles, 427 mAh g^{-1} discharge capacity was observed. Capacity retention of 49 % in total and 94 % between 100 and 1000 cycles was achieved. This value obtained after 1000 cycles effectively shows the h-BN contribution to the Li-S battery capacity thanks to polysulfide adsorption.

To exhibit the polysulfide adsorption effect of h-BN, the static lithium polysulfide adsorption and UV–Vis adsorption tests for 10 h-BN were conducted, as presented in Fig. 7. Static adsorption test was applied to rGO and h-BN/rGO samples in order to reveal the adsorption ability of these samples on polysulfides. (Fig. 7, inset). For this purpose, the samples were kept in Li_2S_6 solution. After 2 h, due to adsorption by h-BN/rGO, the color of Li_2S_6 solution faded significantly, demonstrating the superior LiPSs adsorption ability of h-BN/rGO. In contrast, a weak color change was observed in Li_2S_6 solution after adsorption by rGO. Furthermore, UV–Vis spectroscopy was also used to prove the enhanced the adsorption effect of h-BN/rGO. UV–Vis analysis from the supernatant showed a sharp decrease in the intensity of the characteristic peaks of polysulfides. Compared to rGO, this decrease was greater after adsorption by h-BN/rGO (Fig. 7). As a result, the UV–Vis spectra were taken in the adsorption experiment, which strongly supported the superior adsorption ability of h-BN/rGO on polysulfides [29].

One of the main reasons for the decrease in capacity in Li-S batteries is the formation of polysulfides and their shuttle effect during battery operation. When examining charge–discharge curves, it can be seen that the polysulfide effect is partially mitigated. Graphene-based h-BN composites have been used as host materials in Li-S batteries to prevent polysulfide leakage. Thus, while h-BN's natural adsorption property can adsorb polysulfides, graphene contributes to conductivity and flexibility. The synergistic effect between h-BN and rGO significantly enhances polysulfide adsorption, thereby improving capacity. Additionally, h-BN is a material with mechanical and thermal durability. h-BN provides contribution to capacity preservation by ensuring regular heat dissipation. In order to examine how h-BN, which has this important feature, will have an effect at high temperatures, electrochemical capacity measurements were performed at 50 °C and 100 °C for the 10 h-BN cathode containing 10 % h-BN, which gave the best result. In addition, the electrochemical cell test of the 0 h-BN cathode without h-BN was performed at 50 °C and compared with the result obtained at 25 °C (Fig. 8(a)). Fig. 8(b) shows galvanostatic discharge capacities for the

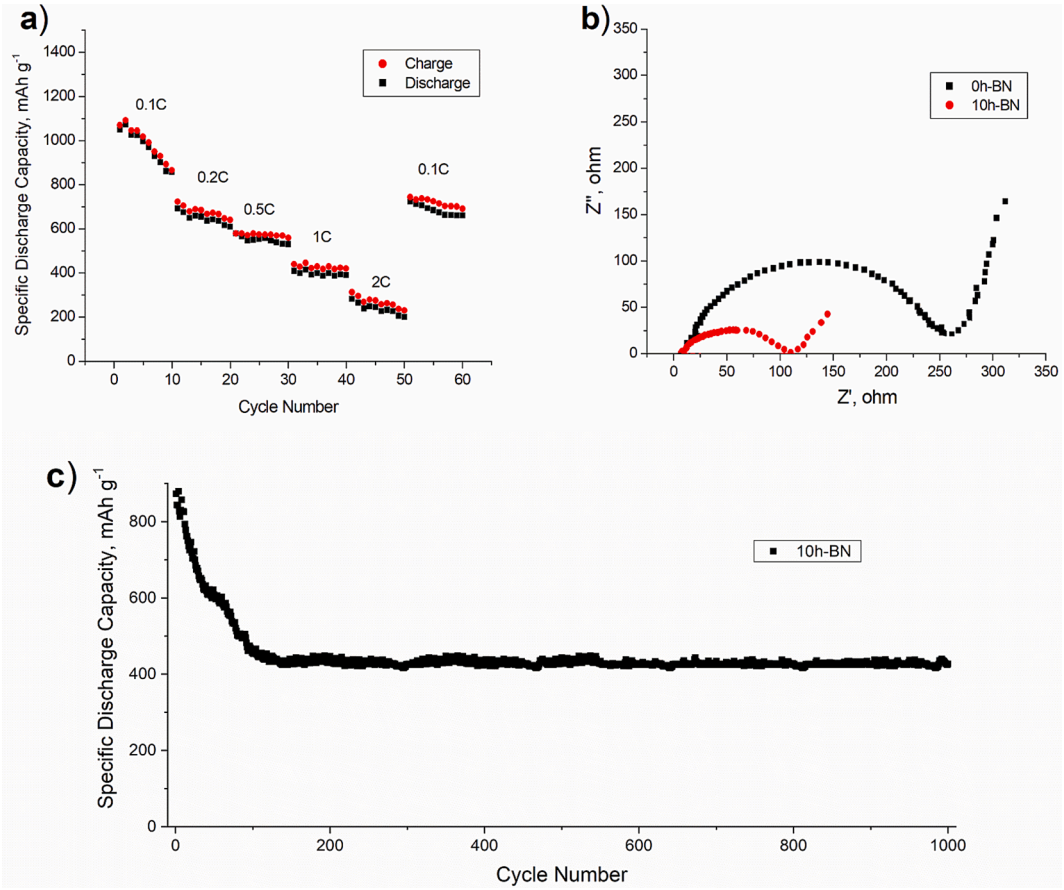

Fig. 6. a) Rate capability of the 10 h-BN cathode. b) EIS Nyquist plots of 0 h-BN and 10 h-BN composite cathodes after 100 cycles charge–discharge testing. c) Long-term cycling perfomance of 10 h-BN at 0.5C.

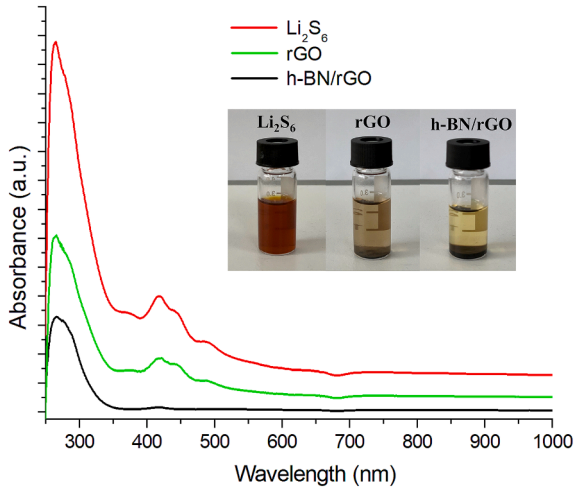

Fig. 7. UV–Vis spectra taken from the Li_2S_6 blank solution and the supernatants after adding h-BN/rGO and rGO, along with inset photographs of the samples.

first cycles at 25 °C, 50 °C, and 100 °C for composite cathodes with h-BN addition. Thus, the effect of h-BN content on the cell capacity under different temperature conditions was investigated. It was observed that the 0 h-BN cathode lost a large capacity with the increase in temperature and the 10 h-BN cathode maintained a higher capacity than room conditions when the temperature increased to 50 °C. Fig. 8(c) exhibits the discharge capacity of 10 h-BN at 25 °C, 50 °C, and 100 °C versus cycle number for 100 cycles. While the first discharge capacity was obtained as 987, 1019 and 750 mAh g^{-1} at 25 °C, 50 °C, and 100 °C, respectively, 724, 792 and 562 mAh g^{-1} discharge capacity was observed at the end of 100 cycles. In this case, 73 % capacity retention was obtained for 25 °C, 78 % for 50 °C and 75 % for 100 °C. In this case, when the temperature was increased to 50 °C, higher capacity values and capacity retention were observed compared to room conditions. At 100 °C, the capacity values were lower and capacity retention was higher compared to room conditions. The result obtained against temperature is consistent with the result put forward by Deng et al. that graphene-h-BN composite is effective in polysulfide adsorption at temperatures between −40 °C and 70 °C [30]. Thanks to the h-BN content, the cycle capability became more stable with increasing temperature. Here, the fact that h-BN provides heat dissipation is effective.

Mussa et al. used h-BN with different rGO contents to increase electrochemical performance of Li-S batteries. They produced composites via a simple microwave hydrothermal synthetic route and formed cathodes by slurry method. After 110 cycles, a reversible discharge capacity of 209.96 mAh g^{-1} with a coulombic efficiency of 86.61 % is observed for the RGO/h-BN/S composite with 70 wt% GO at 0.5C. In addition, they worked at 110 °C and 1C rate for 50 cycles and obtained 123,62 mAh g^{-1} discharge capacity [23]. In this work, we produced h-BN added rGO/S composite cathodes as free-standing electrodes by easy-to-use vacuum filtration method. Binder-free and elactic cathodes were obtained as ready-to-use with no current collector. The cathodes were firstly tested for 100 cycles to determine optimum h-BN content and exhibited as high as discharge capacity of 724 mAh g^{-1} for the 10 h-BN. Then, further electrochemical analyses were conducted for this cathode at higher temperatures for 100 cycles at 0.1C, and long-term cycling test was performed at 0.5C. When compared with the literature, a high discharge capacity of 427 mAh g^{-1} was obtained after 1000

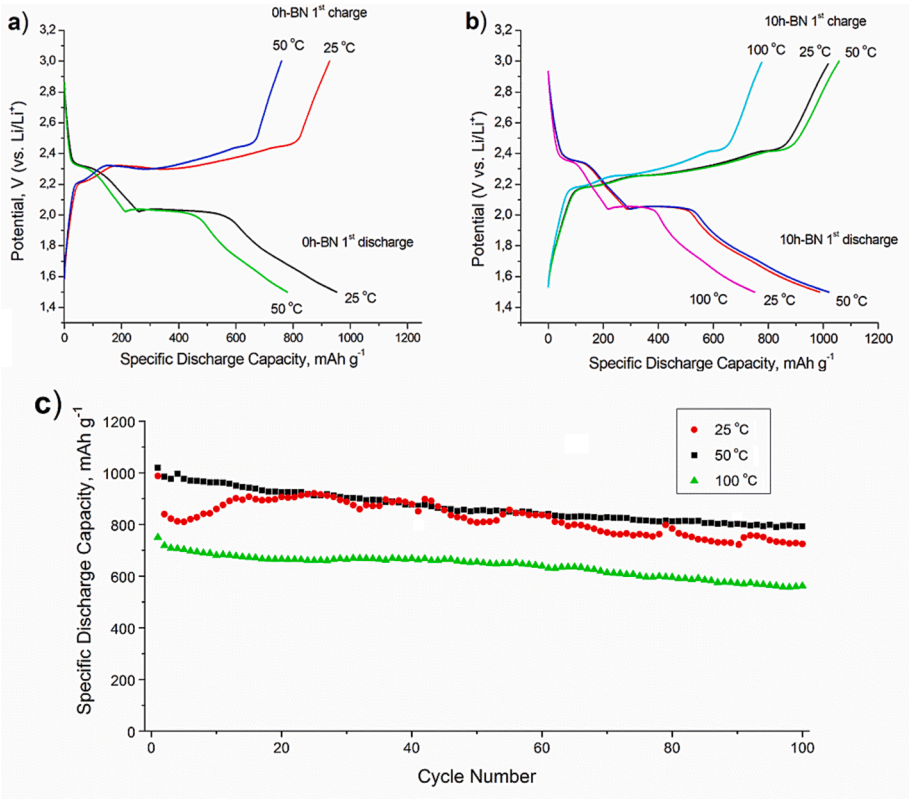

Fig. 8. a) Galvanostatic charge–discharge curves at 25 °C and 50 °C for 0 h-BN. b) Galvanostatic charge–discharge curves at 25 °C, 50 °C, and 100 °C for 10 h-BN. c) Cycling performance of 10 h-BN at 25 °C, 50 °C, and 100 °C for 100 cycles.

cycles.

4. Conclusion

In this study, h-BN/rGO/S composite paper electrode materials containing 0 %, 5 %, 10 % and 15 % wt. h-BN were develeoped as cathodes to improve the characteristics of Li-S batteries and overcome their disadvantages. Our aim in this study is to combine the superior mechanical and chemical properties of h-BN with rGO in the composite film and to show the content and temperature effect of h-BN. When the change in specific discharge capacity for 100 cycles was examined for cathode samples with 0 %, 5 %, 10 %, 15 % h-BN addition, considering both discharge capacity and capacity retention, it was seen that the most suitable h-BN addition belonged to 10 h-BN cathode. Then, long-term cycle test was performed at 0.5C for 10 h-BN and a high discharge capacity of 427 mAh g^{-1} was obtained after 1000 cycles. Further electrochemical analysis was performed for this cathode at higher temperatures for 100 cycles at 0.1C and high discharge capacities of 724, 792 and 562 mAh g^{-1} were obtained after 100 cycles at 25 °C, 50 °C, and 100 °C, respectively. In this case, the cell operating at 50 °C represented 78 % capacity retention after 100 cycles. The polysulfide adsorption ability of h-BN was confirmed by testing with UV–vis spectra taken from Li_2S_6 supernatant. As a result, it has been proven that this composite structure containing h-BN contributes to electrochemical capacity of Li-S batteries by regular heat distribution and adsorbing polysulfides.

CRediT authorship contribution statement

Ayşe Şahin: Writing – original draft, Methodology, Investigation, Formal analysis. **Hilal Günsel:** Writing – original draft, Visualization, Supervision, Methodology, Investigation, Formal analysis, Data curation, Conceptualization, Writing – review & editing. **Şeyma Dombaycıoğlu:** Validation, Methodology, Data curation, Project administration. **Ali Osman Aydın:** Supervision, Project administration, Investigation, Funding acquisition, Conceptualization.

Declaration of competing interest

The authors declare that they have no known competing financial interests or personal relationships that could have appeared to influence the work reported in this paper.

Acknowledgments

This work was supported by the Research Fund of the Sakarya University under Project Number 2020-7-24-60.

Author statement

I Assoc. Prof. Hilal GÜNSEL hereby declare that all the authors agree to submit the paper to Journal of Electroanalytical Chemistry and agreeing with the authorship as well.

References

[1] K.E. Aifantis, S.A. Hackney, R.V. Kumar (Eds.), High Energy Density Lithium Batteries: Materials, Engineering, Applications, 1st ed., Wiley, 2010 https://doi.org/10.1002/9783527630011.
[2] H. Li, R.Y. Tay, S.H. Tsang, W. Liu, E.H.T. Teo, Reduced graphene oxide/boron nitride composite film as a novel binder-free anode for lithium ion batteries with enhanced performances, Electrochim. Acta 166 (2015) 197–205.
[3] C. Zheng, Examining the benefits of using boron compounds in lithium batteries: a comprehensive review of literature, Batteries 8 (2022) 187.
[4] P.J.H. Kim, J. Seo, K. Fu, J. Choi, Z. Liu, J. Kwon, L. Hu, U. Paik, Synergistic protective effect of a BN-carbon separator for highly stable lithium sulfur batteries, NPG Asia Mater. 9 (2017) e375–e.
[5] Z. Wang, J. Shen, J. Liu, X. Xu, Z. Liu, R. Hu, L. Yang, Y. Feng, J. Liu, Z. Shi, L. Ouyang, Y. Yu, M. Zhu, Self-supported and flexible sulfur cathode enabled via

synergistic confinement for high-energy-density lithium–sulfur batteries, Adv. Mater. 31 (2019) 1902228, https://doi.org/10.1002/adma.201902228.
[6] L.K.J. Ting, Y. Gao, H. Wang, T. Wang, J. Sun, J. Wang, Lithium sulfide batteries: addressing the kinetic barriers and high first charge overpotential, ACS Omega 7 (2022) 40682–40700, https://doi.org/10.1021/acsomega.2c05477.
[7] Y. Fan, Z. Yang, W. Hua, D. Liu, T. Tao, M.M. Rahman, W. Lei, S. Huang, Y. Chen, Functionalized boron nitride nanosheets/graphene interlayer for fast and long-life lithium–sulfur batteries, Adv. Energy Mater. 7 (2017) 1602380, https://doi.org/10.1002/aenm.201602380.
[8] E. Kuzmina, E. Karaseva, A. Ivanov, D. Kolosnitsyn, S. Mochalov, R.V. Kumar, V. Kolosnitsyn, Mitigating strategy in lithium dendrite formation in a Li–S cell in accelerated cycling tests, Electrochim. Acta 327 (2019) 135007.
[9] Y. Huang, L. Lin, C. Zhang, L. Liu, Y. Li, Z. Qiao, J. Lin, Q. Wei, L. Wang, Q. Xie, D. Peng, Recent advances and strategies toward polysulfides shuttle inhibition for high-performance Li–S batteries, Adv. Sci. 9 (2022) 2106004, https://doi.org/10.1002/advs.202106004.
[10] Defect-induced-reduced Au quantum Dots@MXene decorated separator enables lithium-sulfur batteries with high sulfur utilization, (n.d.). https://www.oaepublish.com/articles/energymater.2023.76 (accessed January 17, 2025).
[11] Pore filled solid electrolytes with high ionic conduction and electrochemical stability for lithium sulfur battery, (n.d.). https://www.oaepublish.com/articles/energymater.2023.20 (accessed January 17, 2025).
[12] A Separator with Double Coatings of Li4Ti5O12 and Conductive Carbon for Li-S Battery of Good Electrochemical Performance - Xia - 2023 - Advanced Science - Wiley Online Library, (n.d.). https://advanced.onlinelibrary.wiley.com/doi/full/10.1002/advs.202301386 (accessed January 17, 2025).
[13] R. Haubner, M. Wilhelm, R. Weissenbacher, B. Lux, Boron nitrides — properties, synthesis and applications, in: M. Jansen (Ed.), High Performance Non-Oxide Ceramics II, Springer, Berlin Heidelberg, Berlin, Heidelberg, 2002, pp. 1–45, https://doi.org/10.1007/3-540-45623-6_1.
[14] Y. Fu, C. Zu, A. Manthiram, *In Situ* -formed Li_2 S in lithiated graphite electrodes for lithium–sulfur batteries, J. Am. Chem. Soc. 135 (2013) 18044–18047, https://doi.org/10.1021/ja409705u.
[15] M. Öz, Hegzagonal bor nitrürün açık atmosferde termal davranışları, Cumhuriyet Üniversitesi Fen Edebiyat Fakültesi Fen Bilimleri Dergisi 37 (2016) 57–64.
[16] K. Németh, Simultaneous oxygen and boron trifluoride functionalization of hexagonal boron nitride: a designer cathode material for energy storage, Theor. Chem. Acc. 137 (2018) 157, https://doi.org/10.1007/s00214-018-2366-1.
[17] M.M. Rahman, S. Mateti, Q. Cai, I. Sultana, Y. Fan, X. Wang, C. Hou, Y. Chen, High temperature and high rate lithium-ion batteries with boron nitride nanotubes coated polypropylene separators, Energy Storage Mater. 19 (2019) 352–359.
[18] Y. Chen, T. Wang, H. Tian, D. Su, Q. Zhang, G. Wang, Advances in lithium–sulfur batteries: from academic research to commercial viability, Adv. Mater. 33 (2021) 2003666, https://doi.org/10.1002/adma.202003666.
[19] X. Xiong, W. Yan, C. You, Y. Zhu, Y. Chen, L. Fu, Y. Zhang, N. Yu, Y. Wu, Methods to improve lithium metal anode for Li-S batteries, Front. Chem. 7 (2019) 827.
[20] H. Köse, Ş. Dombaycıoğlu, A.O. Aydın, Graphene-based architectures of tin and zinc oxide nanocomposites for free-standing binder-free Li-ion anodes, Int. J. Energy Res. 42 (2018) 4710–4718, https://doi.org/10.1002/er.4223.
[21] Z. Cui, A.J. Oyer, A.J. Glover, H.C. Schniepp, D.H. Adamson, Large scale thermal exfoliation and functionalization of boron nitride, Small 10 (2014) 2352–2355.
[22] H. Köse, B.Ş. Kurt, Ş. Dombaycıoğlu, A.O. Aydın, Rational design of cathode structure based on free-standing S/rGO/CNT nanocomposite for Li-S batteries, Synth. Met. 267 (2020) 116471.
[23] Y. Mussa, Z. Bayhan, N. Althubaiti, M. Arsalan, E. Alsharaeh, Hexagonal boron nitride effect on the performance of graphene-based lithium–sulfur batteries and its stability at elevated temperatures, Mater. Chem. Phys. 257 (2021) 123807.
[24] H. Köse, Ş. Dombaycioğlu, H. Akbulut, A.O. Aydin, Reduced graphene oxide supported tin oxide-boron oxide flexible paper anodes for Li-ion batteries, Turk. J. Chem. 43 (2019) 1244–1257.
[25] D.T. Tran, V.N. Nguyen, rGO/persulfate metal-free catalytic system for the degradation of tetracycline: effect of reaction parameters, Mater. Res. Express 7 (2020) 075501, https://doi.org/10.1088/2053-1591/ab9e47.
[26] C. Sengottaiyan, M. Hara, H. Nagata, H. Mitsuboshi, C. Jeganathan, M. Yoshimura, Large-area synthesis and fabrication of few-layer hBN/monolayer RGO heterostructures for enhanced contact surface potential, ACS Omega 9 (2024) 26307–26315, https://doi.org/10.1021/acsomega.4c02219.
[27] Two dimensional (2D) reduced graphene oxide (RGO)/hexagonal boron nitride (h-BN) based nanocomposites as anodes for high temperature rechargeable lithium-ion batteries | Scientific Reports, (n.d.). https://www.nature.com/articles/s41598-020-58439-z (accessed January 17, 2025).
[28] C. Liu, Z.G. Neale, G. Cao, Understanding electrochemical potentials of cathode materials in rechargeable batteries, Mater. Today 19 (2016) 109–123.
[29] W. Gao, Y. Liu, C. Cao, Y. Zhang, Y. Xue, C. Tang, Boron nitride nanosheets wrapped by reduced graphene oxide for promoting polysulfides adsorption in lithium-sulfur batteries, J. Colloid Interface Sci. 610 (2022) 527–537.
[30] D.R. Deng, F. Xue, C.-D. Bai, J. Lei, R. Yuan, M.S. Zheng, Q.F. Dong, Enhanced adsorptions to polysulfides on graphene-supported BN nanosheets with excellent Li–S battery performance in a wide temperature range, ACS Nano 12 (2018) 11120–11129, https://doi.org/10.1021/acsnano.8b05534.